European Journal of Chemistry

View Journal Online
View Article Online

Metal oxide nanofillers induced changes in material properties and related applications of polymer composites

Murad Qassim Abdulraqeb Al-Gunaid [1,*], Gayitri Hebbur Maheshwarappa [2], Shashikala Badaga Shivanna [3], Mohammed Ali Hussein Dhaif-Allah [4], Waled Abdo Ahmed [1] and Fares Hezam Al-Ostoot [5,*]

[1] *Department of Chemistry, Faculty of Education, Dhamar University, Dhamar, 00967, Yemen*
[2] *Department of Electronics and Communication Engineering, Sri Jayachamarajendra College of Engineering, Mysore, 570005, India*
[3] *Department of Physics, Sri Jayachamarajendra College of Engineering, Mysore, 570005, India*
[4] *Department of Agricultural, Faculty of Agriculture and Veterinary Medicine, Dhamar University, Dhamar, 00967, Yemen*
[5] *Department of Biochemistry, Faculty of Education and Science, Al-Baydha University, Al-Baydha, 00967, Yemen*

* *Corresponding author at: Department of Chemistry, Faculty of Education, Dhamar University, Dhamar, 00967, Yemen; Department of Biochemistry, Faculty of Education and Science, Al-Baydha University, Al-Baydha, 00967, Yemen.*
e-mail: muradal-gunaid@tu.edu.ye (M.Q.A. Al-Gunaid); faresalostoot@baydaauniv.net (F.H. Al-Ostoot).

REVIEW ARTICLE

10.5155/eurjchem.14.3.401-413.2439

Received: 10 April 2023
Received in revised form: 13 May 2023
Accepted: 22 May 2023
Published online: 30 September 2023
Printed: 30 September 2023

KEYWORDS

Band gap
Core-shell NPs
DC-conductivity
Refractive index
Nano-metal oxides
Polymer nanocomposites

ABSTRACT

Nanometal oxides have attracted considerable research interest because of the widespread applications in which nanomaterials can be synthesised in various oxide forms that can adopt various structural geometries with unique electronic band structures. Additionally, nanometal oxides provide unique features imputed to quantum confinement effects that stimulate changes in their optical, electrical, and optoelectronic behaviours. Meanwhile, introducing such nanometal oxides into host polymeric materials enables the formation of advanced polymeric nanocomposites with versatile properties. Even so, the utilisation of such nanocomposites in diverse potential applications requires a fundamental understanding of their inherent material functionalities. Therefore, this document aims to demonstrate the importance of polymer nanocomposites with a special focus on the impact of nanometal oxides to enhance the optical and electrical behaviours of polymer composites for advanced optoelectronic and energy storage applications.

Cite this: *Eur. J. Chem.* **2023**, *14(3)*, 401-413 **Journal website**: www.eurjchem.com

1. Introduction

Today, intercalated polymer nanocomposites (NCs) with nanometal oxides are gaining significant interest in both academic and industrial scenarios. It involves the selection of polymers and metal oxides on the nanoscale from various numbers of polymers and nanomaterials available today for the desired properties. Metal oxides are well-known materials for sensors, photocatalytic, fuel cells, coatings, optoelectronic devices, *etc.* [1-6]. The surface of metal oxides is a key factor for effective interaction with target molecules, however, reducing the size of metal oxide particles to the nanoscale increases the active surface area and induces a new effect due to quantum confinement such as band gap widening, UV-absorption, room temperature, and photoluminescence [7-9]. Compared to traditional spherical nanometal oxide, its excellent electrical properties and unique geometry can increase the bulk conductivity of typical engineering polymers by ~10^{10}-10^{14} S such as resistors, inductors, and capacitors, which are steadily increasing in the electronic industries. The surface of the nanometal oxides provides vacancies orbital's to interact with the host polymers leads to charge transfer between it. The characteristics of individual polymeric nanocomposites are affected by the structure of the components, the content and shape of the nanometal oxides, the morphology of the composites, in addition to the nature of interactions at the interfaces between components in the NC [10,11]. Therefore, the improvement of such properties and interfacial interactions between polymers and nanometal oxides acquire a role in decorated the optoelectrical properties of polymeric nanocomposites. In this chapter, the authors have focused on the effect and role of different nanometal oxides in the modification of the optical and electrical properties of host polymers to be suitable for optoelectronic and industrial applications.

https://dx.doi.org/10.5155/eurjchem.14.3.401-413.2439

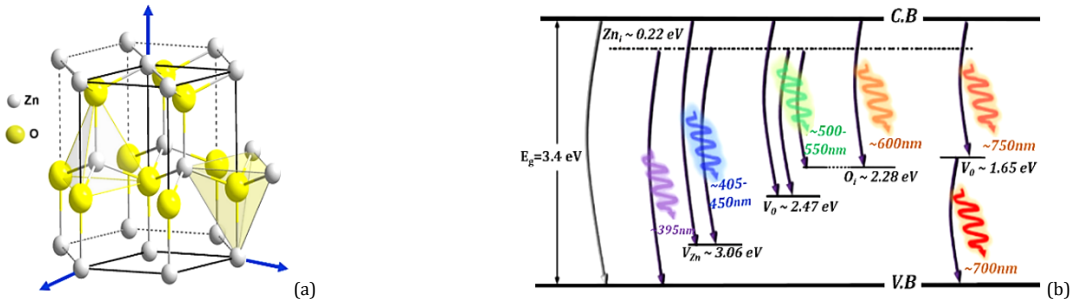

Figure 1. (a) Hexagonal structure and (b) schematic diagram of energy band with some of the defect levels in ZnO structures [24,25].

2. Nanometal oxide features

Nanometal oxide semiconductors are ecofriendly and low-toxic materials with a high surface area, are chemically stable, and exhibit fast electron transfer character, which is required to enhance the performance of nanocomposites. Generally, nanostructured metal oxides, such as ZnO, CuO, NiO, TiO_2, ZrO_2, WO_3, Fe_3O_4, Co_3O_4 and SnO_2, have unique magnetic and super hydrophobic properties. It has different and attractive morphologies such as nanospheres, nanoflowers, nanorods, nanotubes, and nanowires, which convenient and it's important applications such as catalysis, solar energy transformation, gas sensor, magnetic storage media, electronics, electrical and optical switching devices [12-15].

Generally, in the electronic structure of inorganic transition metal oxides, the band gap increases as the ionicity increases, and it may be due to the energy difference between the cation and the orbital of the anion. It implies the splitting of the dangling bond orbital's increases, moving them closer to the band edges. The existence of additional interactions with occupied or unoccupied orbital's (e.g., *d*-orbitals of transition metals) gives rise to secondary bonding-antibonding interactions. Such situations support defect tolerance, since lattice defects (e.g., point defects, grain boundaries) are less likely to create deep defect states within the band gap [16].

In nanometal oxides, optical absorption features are generally affected by 'non-stoichiometry' size-dependent defect effects. Typical point defects in nanometal oxides concern oxygen or cation vacancies and/or the presence of Alien's species, like Cu^{2+} and Ce^{3+} (Alien cations display specific features, such as the localized *d-d* or *f-f* transitions of Cu/Ce). Vacancy defects introduce gap states in proportion to the defect number; in fact, a random distribution of (equal) vacancy defects introduces a Gaussian-like density of states that can produce mid-gap states and/or be localised near the valence and conduction bands depending on the electronic nature (donor/acceptor) of the defect and gives characteristic 'localised' features in the UV-visible spectrum.

Furthermore, metal oxides can exhibit ionic or mixed ionic/electronic conductivity, and it is experimentally well established that both can be influenced by the nanostructure of the solid. The number of electronic charge carriers in a metal oxide is a function of the band-gap energy according to the Boltzmann statistics. Electronic conduction is referred to as (*n* or *p*-hopping type) depending on whether the principal charge carrier is correspondingly electrons or 17 holes. The number of 'free' electrons or holes of a metal oxide can be enhanced by introducing nonstoichiometry and it is balanced by much less mobile oxygen/cation vacancies.

The presence of undercoordinated atoms (like corners or edges) or O valences in metal oxide NPs should produce specific geometrical arrangements as well as occupied electronic states located above the valence band of the corresponding bulk material, enhancing the chemical activity of the system.

The semiconductors including ZnO, TiO_2, and In_2O_3 are well known as n-type transparent conducting metal oxides; however, other main group oxides such as CuO, NiO, MgO, and Al_2O_3 are classified as p-type semiconductors.

2.1. Nano zinc oxide

Among nanometal oxides, ZnO has attracted great attention due to its multiple advantages, such as a direct and wide band gap (3.37 eV) with a large exciton binding energy (60 meV), morphological diversity, and low-cost production. It possesses a hexagonal wurtzite structure with exciting optoelectronic device applications such as light-emitting diodes (LEDs) and efficient laser diodes [17]. The transparent conducting ZnO has native donor defects (n-type semiconductor), where its donor level is often deep inside the band gap, and thermal ionisation can contribute to the n-type conductivity. However, it is challenging in ZnO to achieve p-type conductivity and to develop a p-n homojunction [18,19]. The difficulty may be related to the formation of compensating defects; the low solubility (typically < 10^{18} cm^{-3}) of the acceptor dopants and the high ionisation energy (170-380 meV) of all acceptor candidates [20,21]. Many scientists have been carried out by doping ZnO with other p-type materials, eg, p-Ga N, p-Si and p-type organic materials [22]. The ZnO has a piezoelectric effective, *i.e.*, generate an electric charge in response to applied mechanical stress. In its most common form, the hexagonal wurtzite structure of ZnO has two different surfaces; one is the polar plane and the other is the non-polar plane as shown in Figure 1 [23-25]. The schematic diagram shows the visible emission of ZnO, which is due to the presence of defect levels in ZnO (V_o, V_{Zn} oxygen and zinc vacancies, O_i, Zn_i oxygen, and zinc interstitial). The exits of such point of defects in the crystal structure are exploited for optoelectronic devices [23].

2.2. Titanium oxide

Nanosized titanium oxide (TiO_2) is considered a nearly perfect material due to its remarkable and unique optical properties. It is another n-type semiconductor with a wide band gap ranging from 3.2 to 3.6 eV. The so-called "quantum confinement" or "quantum size effect" is restricted in TiO_2 to very low sizes, below 10 nm, due to its rather low exciton Bohr radius. The Ti-O bond appears to have an increasing covalent character with the oxygen content of the oxide, so the departure of Ti^{n+} from the formal oxidation state increases from + 2 to + 4. TiO_2 NP can be used in several potential applications such as chemical sensors, solar cells, catalysis, magnetism, dielectric materials for ultrathin film capacitors, optoelectronic devices, cosmetics and biomedical fields [26,27]. The chemical and physical properties of TiO_2 depend on its microstructure, such as the morphology, size, and orientation of the constituent grains.

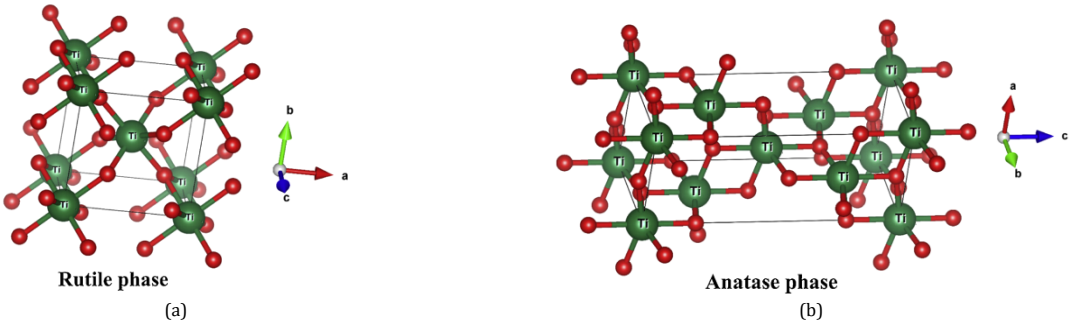

Figure 2. (a) The rutile and (b) anatase phases of TiO_2 structure [31].

Figure 3. (a) Monoclinic unit cell and (b) TEM micrographs of CuO structure [34,35].

Uniform-sized TiO_2 NPs with diverse morphologies were successfully synthesised by different methods such as hydrothermal, sol-gel, chemical precipitation, and microwave-assisted methods [28,29]. There are three different polymorphs of TiO_2 NP known as anatase, rutile, and brookite structures. Figure 2 displaces the rutile and anatase phases of TiO_2 NP. The anatase phase has a higher density of localised states, leading to higher photocatalytic activity compared to other crystalline forms [30,31]. In TiO_2, the oxygen vacancy defect state is created predominantly by the Ti-*d* orbitals. Therefore, the electronic behaviour of the V_O (oxygen defect) is strongly influenced by the propensity of Ti to assume a Ti ion oxidation state when the Fermi level lies close to the conduction band of TiO_2.

2.3. Copper oxide

Copper oxide (CuO) is a native p-type semiconductor with an indirect narrow energy band gap of 1.2-1.9 eV and a refractive index of around 2.63. It is a suitable material for high-efficiency solar cells, because their direct band gaps are close to the ideal energy gap for solar cells and well matched with the solar spectrum. CuO has been used as a hole transfer layer and a barrier layer for dye-sensitive solar cells [32]. Figure 3 shows the monoclinic crystal structure and CuO TEM image that has the space group 2/m or C_{2h} and lattice parameters of 0.468 nm, 0.342 nm and 0.513 nm, at β = 99.55° [33-35]. It has a unique monoxide as a square planar coordination in a unit cell where the copper atom is surrounded by four oxygen atoms in the configuration [33]. CuO NPs are nontoxic and have a low production cost, high surface area to volume ratio, good electrochemical activity, and electron transfer at lower potential. It can be synthesised in different shapes by various techniques such as hydrothermal, sol-gel, and combustion methods.

The unique features of CuO NPs make it suitable for many technological fields such as active catalysts, gas sensor, magnetic recording medium, and high critical temperature superconductor [36,37]. Raman spectra of different grain sizes CuO NPs at different temperatures revealed that the intensity of the spectrum is related to the size of the NPs, where the smaller NPs showed stronger and sharp peaks and shifted to smaller wave numbers, which may be explained by the phonon confinement effect in nanometre-sized materials. The number of crystal defects increases rapidly as the size of the NPs decreases due to the large surface/volume ratio and the contribution of the vibration of oxygen atoms [38,39]. Besides, the luminescence of CuO NPs is generally supposed to show the existence of defects, where the deep emissions may be due to the existence of Cu vacancies, which are the most stable defects in CuO. However, the formation energy of oxygen vacancies or interstitial defects (O, Cu) is not much different from the formation energy of Cu vacancies [40].

2.4. Nickel (II) oxide

It is another native p-type *3d* transition metal oxide semiconductor with small size (< 100 nm). Nickel (II) oxide (NiO) NP has multifunctional properties, such as wide band gap (~3.88 eV), specific capacitance (~390 F/g), high discharge capacity (~638 mA h/g), high carrier density (~7.35 - 1018 cm^{-3}), and photon to current conversion efficiency (~45%), in addition to excellent catalytic activity (42.3 gm^{-2}) for CO oxidation. It shows good electrical, electrochromic, and thermo-electric properties as well as high chemical resistance. Therefore, NiO NPs are a highly desirable candidate for applications in electronics, electrochemical devices, photovoltaics (PVs), sensors, and catalysis [41,42]. The crystal structures of NiO are commonly known as a cubic rock salt structure; the nickel atom is placed in a six-fold octahedral coordination, as shown in Figure 4, along with the TEM image of NiO NPs [43,44].

Among several different approaches to produce NiO NPs, hydrothermal method is the fever is technique for growing the NiO NPs due to inexpensive apparatus, low temperature operation, and it is substrate independent. However, the hydrothermal method produces impure NiO material as a result of the hydroxide produced in the growth solution. The impure NiO NPs was annealed at 300-500 °C to produce its pure nanostructured phase [45].

(a) (b)

Figure 4. (a) Cubic rock phase and (b) TEM micrographs of NiO structure [43,44].

2.5. Tungsten oxide

Nanosized tungsten trioxide (WO_3) is one of the transition metal oxides that is known to be an important p-type semiconductor with a bandgap of 2.5-3.0 eV. The crystal structure of WO_3 can be orthorhombic, hexagonal, tetragonal, or monoclinic. It has several potential applications, such as electrochromic windows, information storage media, optical devices, photocatalysts, and gas sensors [46]. Much effort has been exerted to synthesise WO_3 NPs in different nanostructurer shapes (nanotubes, nanowires, nanoplatelets, etc.) by various techniques [47,48]. The synthesis of WO_3 NP as hollow spheres can be adjustable by calcinating acid-treated $PbWO_4$ and $SrWO_4$ at 500-600 °C for 2 hours [49]. Furthermore, tungstic acid ($H_2W_{15}O_{55}{\cdot}H_2O$) hollow spheres and nanotubes have been synthesised via a nonaqueous and surfactant-free through solvothermal reaction for WCl_6/urea/ethanol system in the presence of WO_3 and subsequent slow calcination [50]. The Hollow structure of WO_3 resulting nanoporous walls make it as a promising material for energy storage fields, catalysis and bio-technology applications.

3. Polymer nanocomposites

Today, within the limits of materials technology, the concept of mixing different types of materials through synergy is one of the most effective ways to achieve specific objectives with the highest efficiency in properties and cost-effectiveness. Therefore, significant efforts have been made to control the nanostructures via innovative synthetic methods. The features of nanocomposites (NCs) depend on the nature, composition, and properties of nanomaterials with their morphology and interfacial characteristics. It can be widening the application window of the NCs by an optimised fabrication process and controlled nanosized dispersion, thermal stability, and mechanical properties such as toughness, hardness, adhesion resistance, and flexural strength. The high volume-to-surface and aspect ratios of nanometal oxides (nanoparticles) make it highly preferred to utilise it as a filler in polymeric matrices. Generally, solution casting, melt mixing, and in situ polymerisation approaches have been used to fabricate polymer-based NCs.

In solution casting, the polymeric matrix completely dissolves in a suitable solvent, and then the nanometal oxide will be homogeneously dispersed in the solution by ultra-sonication followed by evaporation of the solvent to a typical dry film forming. The solvent assists in the segmental motions of the polymeric chains which lead to perfectly dispersive nanometal oxide inside the polymeric chains. Whereas melt blending needs a high processing temperature, it does not require solvent as an intermediate between nanometal oxide and polymer, where both components are added to the extruder with intensive mixing for some time, and the NCs come out of the die. The mobility of polymeric chains simply comes from thermal energy. However, in the case of in situ polymerisation, the monomer and nanometal oxide are mixed initially. Monomers are allowed to disperse between nanometal oxide particles, where monomer polymerisation may occur on the surface of nanoparticles (NPs) as a core-shell or coating on the NPs [51-53]. Figure 5 shows the steps of some approaches to the preparation of polymer-based NC films. The content of nanometal oxide has a high impact on the properties of polymer NCs where the interparticle distances are small and the conversion of a large fraction of the polymer matrix near its surface into an interphase of different properties as well as a change in the morphology [54-57]. At lower doses of nanometal oxide, the uniform dispersion of particles in NCs can occur. In addition, the geometrical shape of the nanoparticles plays an important role in determining the properties of NCs.

Furthermore, the preparation of high-quality polymer NCs containing high nanometal oxide content has faced common problems which represent barriers to the development of polymer NCs, such as dispersion, the interface between NP and polymer, alignment of NPs and quality of nanostructures [58]. A homogeneous dispersion of NPs is crucial in polymer-NCs. Agglomeration may occur in poorly dispersed NPs creating micron-sized aggregates. Air may trap inside the aggregates which may cause void within NCs lowering its properties [59]. Modifying the surface of NPs may be needed to improve their dispersion in the polymeric solution, which is important to maintaining transparency after the formation of NC films. As presented in Figure 6, organo-silane compounds like ($RSi(OMe)_3$ (R = 3-Methacryloxypropyl)) have been used successfully to modify the surface of Al_2O_3 NP [60]. In addition, carboxylic acids, phosphorus coupling reagents, and surfactants have generally been utilised for surface modification of TiO_2, ZnO, Al_2O_3 and SiO_2 NPs to reduce their aggregations, which enhances their uniform and stable dispersion in the polymers [61-64]. In addition, physical treatment may also help in the dispersion of NPs where physical mixing devices such as ultrasonication, shear mixing, and ball milling are also used.

4. Optical behaviours

4.1. Absorbance and band gap energy

Interestingly, in all NC materials, the optical properties are closely related to the structural properties, compositional parameters, vacancy density, and dopant level. The UV-vis spectrum is an important tool for understanding the band gap structure, electronic properties, and optical constants (refractive and absorption indices) of pure and doped polymers. The data of the absorption curve in the lower energy part provide information about atomic vibrations, while the higher energy part of the spectrum gives knowledge about the electronic states.

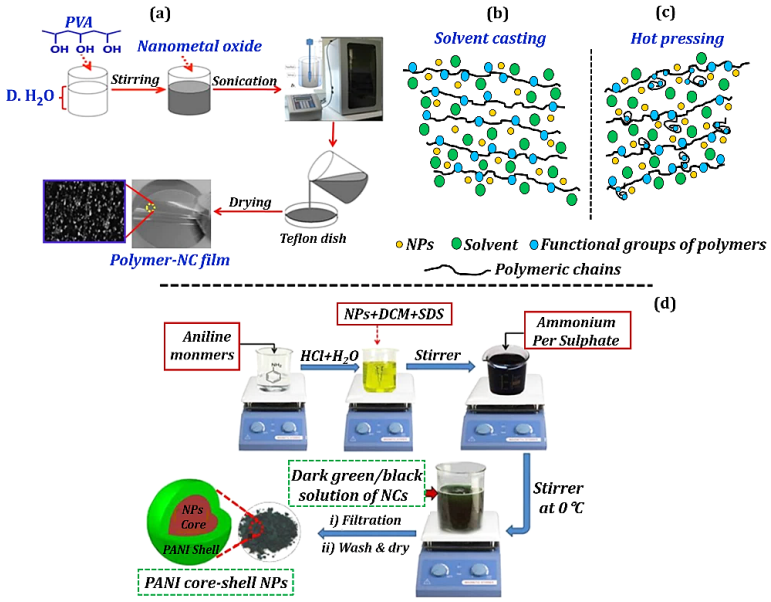

Figure 5. Schematic diagrams of; (a) Fabrication of PVA-NC film by solution casting; (b) and (c) NC films by solution casting and hot pressing and (d) PNI and PANI core-shell NPs through in-situ polymerization by chemical oxidation method [56,57].

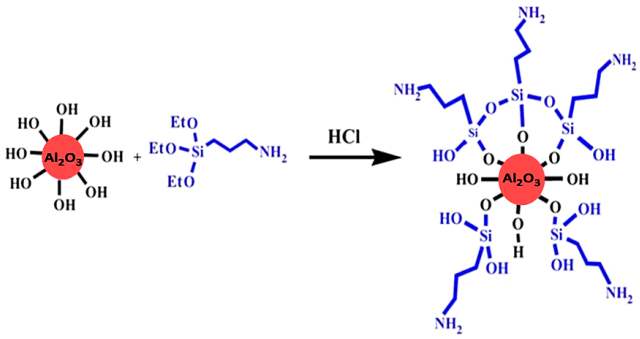

Figure 6. Schematic represents the modification of Al_2O_3 NPs with silane compound [60].

There are numerous polymers such as poly(vinyl alcohol) (PVA), PMMA, PVDF, PVP, PS, PC; *etc*. can be used as a matrix in NCs due to their unique properties such as flexibility, high transparency in the visible region, thermal capability, excellent mechanical properties, low cost, low refractive index, and easy film formability and process ability. Typically, these transparent polymers have low response towards the absorption of incident light and it has high band gap energy, E_g, normally it lies in the range 5.0-6.5 eV.

Optical materials with lower E_g and higher refractive index (n) values are rapidly utilised because of the urgent demands imposed by the development of advanced photonic and electronic devices like solar cells, light-emitting diodes (LED and organic LED), optical lenses and filters, anti-reflexion films and optical adhesives.

For achieving such objectives, nanometal oxide having suitable features such as E_g and/or n is incorporated into polymeric matrices. Significant enhancement in the optical properties of polymers can be achieved even with a small dose of NPs. The dispersion of NPs inside the host polymer leads to the formation of an intermediate state in its band-gap level. So, the electrons (existence in the functional groups of the polymeric matrix) are first based on the absorption of incident light and transition from the VB to the intermediate state in the band-gap level, and then promoted by photons of incident light from the interband to the CB. This process can be detected by the shift of the absorption edge (in the absorption curve) of the NC compared to the pristine matrix due to a temporary increase in the carrier density among the NCs, which in turn alters its properties [65].

Generally, the value and nature of E_g depend on the linear absorption coefficient, α, of the materials and E_g can be determined using the equation as follows;

$$(\alpha h\upsilon)^m = A\left(h\upsilon - E_g\right) \quad (1)$$

Where α is the linear absorption coefficient, m is the frequency or index that describes the optical absorption process, h is the Planck constant, and A is a constant that depends on the probability of transition. Theoretically, m is equal to 2 for direct allowed, 2/3 for direct forbidden, 1/2 for indirect allowed, and 1/3 for indirect forbidden transition. The value of m decides the nature of the E_g or the transition involved. Through the literature [66-68], the index m can be practically obtained, which depends on the value of α by taking the slope of the graph between *log* (α) and *log* ($h\upsilon$). The value of index m, which gives the best linear graph, is chosen. Using the Tauc graph, the value of E_g estimated from the graph of $(\alpha h\upsilon)^2$ *versus* ($h\upsilon$) and extrapolating the linear portion of the curve to the $h\upsilon$-axis.

Interestingly, in all NC materials, the optical properties are closely related to the structural and compositional parameters, the vacancy density, and the level of dopants.

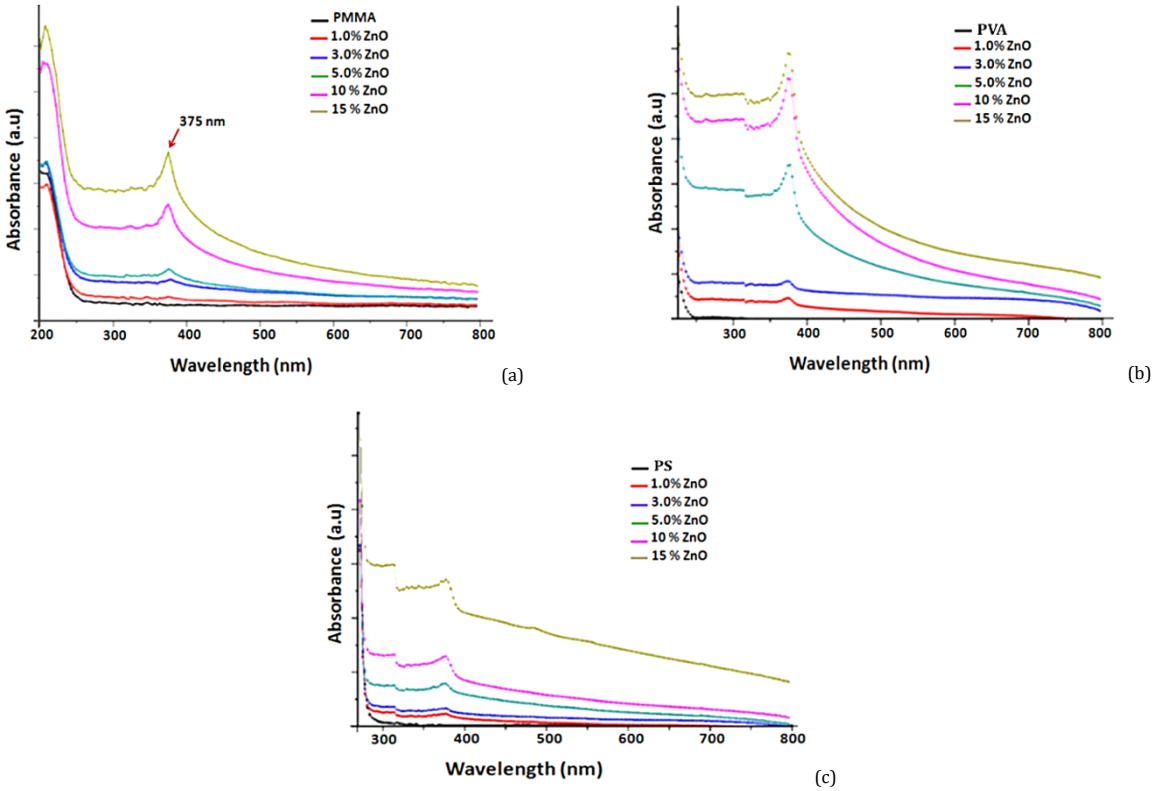

Figure 7. Absorbance of (a) PMMA/ZnO, (b) PVA/ZnO and (c) PS/ZnO NC films [70].

The UV-vis spectrum is an important tool for understanding the band gap structure, electronic properties, and optical constants (refractive and absorption indices) of pure and doped polymers. The data of the absorption curve in the lower energy part provide information about atomic vibrations, while the higher energy part of the spectrum gives knowledge about the electronic states.

On the basis of the above, the flexible foil of NCs based on polymer/ZnO has been successfully developed by the casting method to investigate the optical and electrical properties. Quadri *et al.* (2017) [69], reported that ZnO NPs have a significant effect toward UV-Vis absorption after incorporated into selected polymers such as PEG, PVP, and PAN. Such pure polymers have π absorption appearing at 245-275 nm referring to the functional groups in their structures. NCs based on ZnO/PEG, ZnO/PVP, and ZnO/PAN displayed new characteristic absorption peaks at 368, 367, and 372 nm, respectively, attributing to the presence of ZnO NPs, which has a characteristic peak at about 360-380 nm. The existence of these peaks confirms the formation of the NCs.

The optical performance of NC films containing different weight fractions of ZnO NP embedded in PMMA, PVDF, PVA, and PS were also studied [70]. Figure 7 illustrates the optical absorption of the selected polymer/ZnO NCs [70].

The transparency of pristine polymers was in the order as; PMMA > PVA > PS, whereas PVDF showed the lowest transparency in the UV and visible regions. As the dosage of ZnO NPs increased, the percent of transmittance of all NC films was reduced. The absorption peak of all NCs was observed in the 370-377 nm wavelength range, indicating the effect of ZnO NPs on polymeric matrices. However, NC films exhibit high transparency at > 400 nm due to the lower absorption of ZnO NPs in the visible region. Such trends may have been explained by the smoothness of the surface, which increases the reflectivity or light scattering by the individual ZnO NPs, leading to lower transmittance values in the visible range. Furthermore, the optical band gap energy (E_g) was reduced for pure PMMA, PVDF, PVA, and PS (5.08, 5.88, 5.25 and 4.5 eV) to their corresponding NCs (4.5, 5.1, 4.75 and 3.9 eV) doped with 15 wt% ZnO.

The reduced in E_g value denotes the shift of the VB and the CB which can be noticed in Tauc's plot by the displacement position of absorption edges in NCs as compared to pure polymers. The increase of carriers in VB and CB and the presence of unsaturated defects leads to an increase in the density of localised states in the band gap of the matrix, leading to a reduction in its E_g.

In this regard, the pioneering report demonstrated that the existence of ZrO_2 NPs within the PVC matrix modified the optical properties due to the wide E_g (5.17 eV) of ZrO_2 NPs. Pure ZrO_2 NPs have a sharp and intense band at 212 nm with an absorption edge around 300 nm [71]. Mallakpour *et al.* [72,73] modified the surface of ZrO_2 NP with vitamin B1 and bovine serum albumin (BSA) to achieve excellent dispersion and improve the interface between ZrO_2 NP and the PVC matrix (Figure 8). Pure PVC has two adsorption peaks at 225 and 280 nm assigned to $\pi \rightarrow \pi^*$ and $n \rightarrow \pi^*$ transitions, respectively. The intensity of both PVC/ZrO_2-vitamin B1 and PVC/ZrO_2-BSA NCs increases with a higher red shift of the absorption edge up to ~ 450 nm. The E_g of PVC was reduced from 5.56 eV for pristine PVC to 4.4 eV for PVC doped 6 wt% ZrO_2-BSA. Beyond this, Taha *et al.* [74] reported that introducing 0.5wt% of NiO NPs into PVC improves the absorption process of NCs and reduces the E_g to 5.15 eV. Furthermore, Shashikala *et al.* [75] revealed that the embedded of 4wt% of poly aniline core-shell halloysite nanotubes (HNTs) into PC matrix, promotes the absorption of NCs in the UV-visible region as well as decreasing E_g to 2.87 eV. The reduction of E_g into 3.25 eV for a natural gelatin matrix containing 4wt% of poly *o*-anicidine encapsulated K_2ZrO_3 NPs has been mentioned by Anupama *et al.* (2022) [76].

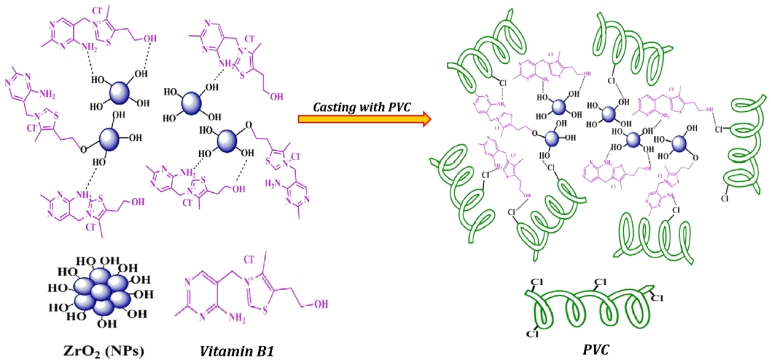

Figure 8. Schematic representations of modified ZrO_2 and ZrO_2-vitamin B1/PVC NCs [72].

The pioneering reports demonstrated that the PVA matrix is more suitable compared to other polymers, where it can be modified the band-gap energy and response toward incident light for even further. Al-Hakimi *et al.* [77] concluded that the mixture of TiO_2/Cu NPs induces the UV-visible radiation absorption process in the PVA film, where a new broadening and intense peak appears at 397-516 nm. The optical E_g of PVA was found to decrease from 5.2 to 3.5 eV with increasing the concentration of TiO_2 up to 2.5 wt% in the PVA matrix. While the further decrease in the band gap of PVA film to 3.12 eV after doping by 1.6 wt% TiO_2/Cu NPs was also noticed [78]. Similarly, Li *et al.* [79] demonstrated that the PVA/WO_3 NC films showed a strong absorption band around 300 nm and a broad absorption with a maximum peak of approximately 590 nm that was accompanied by a reduced band gap of 1.81 and 1.82 eV of the sample with 0.6 and 1 wt% WO_3, respectively. Meanwhile, Selvi *et al.* [80] evaluated the influence of p-type CuO NPs, which improves the inherent properties PVA films and observed a new peak at ~350 nm, whereas the E_g obtained is 4.64 eV for PVA containing 6 wt% of CuO NPs. However, Abdullah *et al.* [81] illustrated that the increased dosage of CuO NPs between 10-12 wt% in the host PVA leads to the appearance of an additional broad absorption peak between 580-840 nm, which is due to surface plasmon resonance (SPR) of CuO NPs which also gives an intense colour to the PVA films. The minimum E_g value observed is 3.18 eV for PVA-12 wt% CuO NPs, which indicates to modify the electronic structure of the PVA matrix. This means that the CuO NPs may form localised electronic states in the E_g of PVA which act as trapping and recombination centres, leading to a reduced E_g of PVA in NC film. Recently, nanometal oxide NPs had been hybridised by multielements to further improve their features, which in turn can be more effective in modifying the properties of the polymeric matrix. Murad *et al.* [82] reported that the addition of a small amount (2 wt%) of hybrid La_2CuO_4 NP has a higher impact on the performance of PVA to absorb UV-visible light, where the intensity of absorption peaks becomes high in addition to the shoulder peak having been observed at 312 nm, while the E_g value was reduced to 3.2 eV for PVA/2 wt% La_2CuO_4 NC film. Similar trends in reducing E_g values were also observed for PVA/2.5 wt% $AgAlO_2$ and PVA/8 wt% $CaNiAl_2O_5$ NPs, where the minimum E_g values achieved are 2.78 and 2.80 eV, respectively [83,84].

4.2. Refractive index

The refractive index, *n,* plays an important role in optical communication and in the design of optical devices. High-refractive-index polymers (HRIPs) have drawn a great deal of scientific interest due to their potential applications in optical filters, waveguides, lenses, light-emitting diodes (LEDs) and reflectors [85]. However, the optical application of conventional polymers is limited due to their narrow range of refractive indices, *n,* which in general < 1.8. Nanometal oxides, on the other hand, have a broad *n,* but suffer from weathering effects. Thus, the fabrication of polymer NCs combines the lightweight and cost-effective features of the polymers with the high *n* and UV-radiation shielding abilities of the NPs. Generally, *n* can be estimated using the equation as follows;

$$n = \frac{1+R}{1-R} + \sqrt{\frac{4R}{1-R^2} - K^2} \quad (2)$$

Where K is the extinction coefficient ($K = \alpha\lambda/4\pi$). R is the reflectance (R = 1-A-T; where A is the absorbance and T is the transmittance). The n for NCs can be modified by changing the concentration of NPs, as its dispersion inside the polymeric chains has an important effect. Through a literature survey, the finer dispersion and higher penetration of NPs among polymeric chains caused a good interaction with the functional groups in the polymer via a dipole-filler interaction or charge transfer complex (CTC). It leads to an increase in the packing density in NC, therefore, n tends to increase [86,87]. In addition, n denotes to polarizing of molecules (dipoles and NPs) by the electromagnetic field of light. The polarisation molecules will interact with incident light, where these types of molecules have more ability to reduce the speed of light that passes through the polymer network. Therefore, the polarisation strength will be higher inside NC films as the NPs content increases, resulting in more interaction with the electro-magnetic field of the incident light. It causes an increase in the absorption process, hence an increase in n according to the Lorentz-Lorenz formula [88,89].

A number of high *n*-value semiconducting NPs such as ZnO and TiO_2 have been studied as additives to increase the n of polymer matrices. Since the n of PMMA is relatively low for optical applications (n = 1.49), incorporation of ZnO NPs in PMMA to prepare transparent NC films via evaporative ligand exchange of hybrid particle fillers has been investigated by Wang *et al.* [90]. The n of the hybrid film increased to 1.65 with higher ZnO NPs contents of up to 38 wt%. Yuwono *et al.* [91] demonstrated that introducing TiO_2 NPs into PMMA to obtained NC films via the *in situ* sol-gel route leads to an increase in n to 1.780 for PMMA/60mass % TiO_2. The homogeneous dispersion of TiO_2 NP in PMMA is one of the important issues in the fabrication of transparent TiO_2 / PMMA NCs, the suppression of Rayleigh scattering at the interfaces between inorganic components and polymer matrices. It is required to maintain the transparency after the formation of NPs in the polymer matrix. TiO_2 NPs easily aggregate in hydrophobic polymers such as PMMA and PC matrices due to its surface being covered with hydrophilic hydroxyl groups.

Table 1. Refractive index of some NC films.

Matrices	NPs	% NPs	Methods	RI (*n*)	Reference
P-4-VBA *	TiO_2	60	In-situ polymerization	1.77	[93]
Epoxy	TiO_2	20	Simple and efficient way	1.73	[94]
PVP	$CsAlO_2$	8	Solution casting	2.64	[95]
PVP-PVA	ZnO	5	Solution casting	2.01	[96]
PVT/DVB *	ZrO_2	61.5	In-situ polymerization	1.71	[97]
PC	PANI+$NaBiO_2$	4	Intercalation method	2.53	[98]
Gelatin	K_2ZrO_3	4	Solution casting	2.38	[99]
PVA	ZrO_2	80	A spin-coating process	1.75	[100]
PVA	$AgAlO_2$	2.5	Solution casting	2.44	[83]
PVA	$ZnBi_2MoO_7$	8	Intercalation method	2.14	[101]

* P-4-VBA is poly(4-vinylbenzyl alcohol), PVT/DVB is a copolymer of (trans-β-methylstyrene and divinylbenzene).

Modification of the surface of TiO_2 NP with oleyl phosphate (OP) to enhance the optical properties of TiO_2 / PMMA NC reported elsewhere [92]. The *n* of the OP-modified TiO_2/PMMA NCs containing 20 wt% of TiO_2 changed to 1.86. The data of *n* values for various nanometal oxide doped different polymers are tabulated in Table 1.

5. Electrical behaviors

Improvement of advanced materials based on poly(vinyl chloride) (PNC) that exhibit multifunction features is one of the most important challenges in a widening of its applications. Therefore, in addition to reducing the optical bandwidth and enhanced refractive indices with retaining high optical clarity, it is required to achieving good electrical properties of polymers at room temperature as well as a lower dosage of NPs. Conventional host polymer incorporated nano-metal oxide demonstrates an advanced enhancement in electrical conductivity. In NC films, the conduction is due to the motion of electrons in the conduction band and holes in the valence band or hopping of the carrier between localised sites in the polymeric matrix. The energy required for electronic conduction can be supplied by the applied electric field to excite a carrier, and this hopping process is favoured in the case of highly disordered NC films. In addition, dielectric films differ in their electrical properties according to the preparation parameters. The electrical properties of NC films depend upon their microstructure and are strongly linked to the nano-structure of the particles, particularly the distance between the particles in the polymeric matrix.

Ma *et al*. [102], reported that PS resin/ZnO NCs were prepared by melt-blending. Surface resistivity decreases as the amount of ZnO increases. PS doped with 30% wt% ZnO spherical and whisker particles reduced the surface resistivities from 1.0×10^{16} to 8.98×10^{12} Ω/cm² and 9.57×10^{10} Ω/cm², respectively. The amount of ZnO in the PS resin can gradually increase to form a conductive network. Maji *et al*. [103], inspected that PMMA reinforced with silane-modified ZnO NCs was synthesised via in situ polymerisation technique. Incorporation of m-ZnO into the PMMA matrix significantly improved ac-conductivity (σ_{ac}) to ~ 3×10^{-4} S/m at 323K, while the dielectric constant increased to (ε' = 81) compared to unmodified ZnO (ε' = 10). The conduction transport occurred due to the large polaron-assisted tunnelling mechanism. Morsi *et al*. [104], investigated the effect $BaTiO_3$ embedded in PEO/CMC was prepared by a solution casting technique. The data showed enhances σ_{ac} and reached 1.8×10^{-7} S/m at room temperature for 0.32wt% $BaTiO_3$ doped in PEO/CMC. The ε' is increased to ~58 compared with <10 for pure blend. The increase σ_{ac} is may be due to increases in the contents of $BaTiO_3$, whose interactions with PEO / CMC promote the charge conduction mechanism.

The electrical conductivity of PVA/PVP blend (50:50) and its NCs with different contents of MoO_3 NPs have been studied by Rajesh *et al*. [105]. The conductivity is increased from 7.19×10^{-8} S/cm for the pure blend to 5.49×10^{-7} S/cm for PVA/PVP blend with 12 wt% MoO_3 NPs. This composite exhibited higher ε' ~48 which may be referred to Maxwell-Wagner polarisation. This type of polarisation arises due to conductor-insulator interfaces. The build-up of space charges or dipoles at the interface electrode polarisation effect leads to increase ε'.

The dependence of σ_{ac} with frequency and content of NPs for NCs based on PVA/ZnO-Ce_2O_3 was discussed by Chandrakala *et al*. [106]. The σ_{ac} increases with increasing frequency and mobility of charge carriers in the NCs, where the highest σ_{ac} obtained for PVA/2wt%ZnO-Ce_2O_3 is $\sim1.1\times10^{-5}$ S/cm. The dependence of σ_{ac} with frequency can be divided into three distinct regions, implying the existence of different dissipated patterns. In the high-frequency region (I), the conductivity increases with increasing frequency. In the low-frequency region (III), a levelling off of the electrical conductivity is observed. In the intermediate region (II), a dipolar relaxation process is present, the intensity of which is independent of the filler content. Similarly, the introducing 8wt% $CaNiAl_2O_5$ NPs into PVA matrix raised the optimum σ_{ac} value to 3.2×10^{-5} S/cm accompanied with enhance ε_{max} to 134 [84].

5.1. Current-voltage (I–V) characteristics

As is known, to understand the direct current conductivity (σ_{dc}) behaviour of PNCs, the current-voltage (*I-V*) behaviour was measured and plotted. From the literature [107-109], the flow current, *I*, in PNC films is strongly dependent on the applied voltage, *V*. When the *V* was increased, *I* increased gradually at first and then increased drastically; this result indicated non-Ohmic behaviour. Figure 9a shows the normal current-voltage (*I-V*) characteristics of pure PVA and doped with different ratios of $CaAl_2ZnO_5$ NP.

In Figure 9a, two distinct regions can be discerned that appear at lower and higher voltages. Gayatri *et al*. [110], illustrated in the lower voltage region, the flow current in PVA/$CaAl_2ZnO_5$ NCs is very low, suggesting that Ohmic is the dominant mode of conduction. At a lower dosage of the NP content in the PVA matrix, the resistivity may arise, restricting the increase of electrical current through the NC film. That initial resistivity at lower voltages may refer to the Coulomb blockade effect. Such phenomenon will occur after the addition of a small amount of NPs into the polymer, referring to the fact that many tunnelling knots may be formed, preventing the electron/charge carrier from moving directionally in a certain electric field. Rozra *et al*. [111], reported that the resistance of PVA/Cu NCs decreases with increasing NP contents due to the distance between the NPs being reduced at higher doses. At higher voltage, the electrical field is large enough to induce the electrons to tunnel from one particle to another, which leads to an increase in conductivity. In addition, increasing the NP content in the PVA matrix enhanced the formation of a network bridge because of the higher probability of physical contact between charge carriers. This contact could form a conduction path, which may have resulted in an increased *I*.

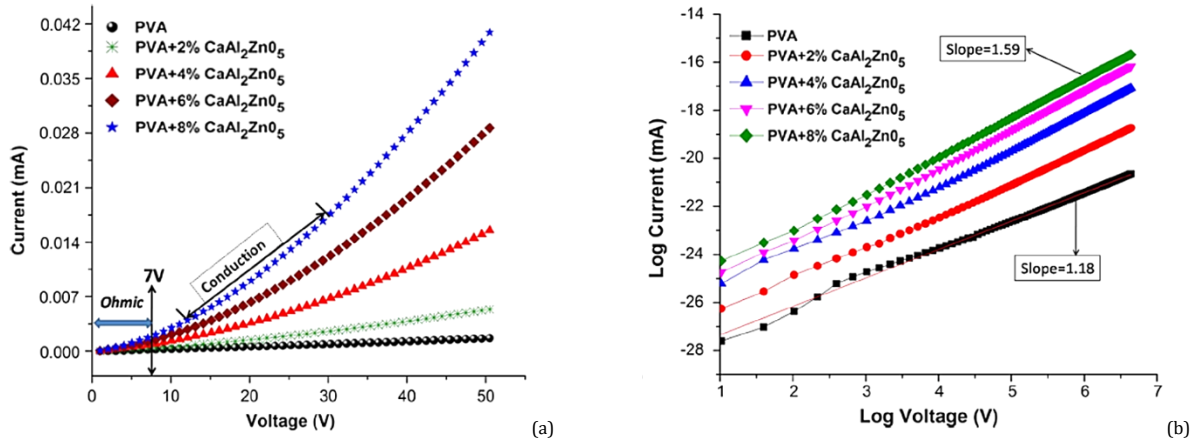

Figure 9. Plots of; a) Current-voltage (I-V) and b) Log (I-V) for PVA/$CaAl_2ZnO_5$ NCs at room temperature [110].

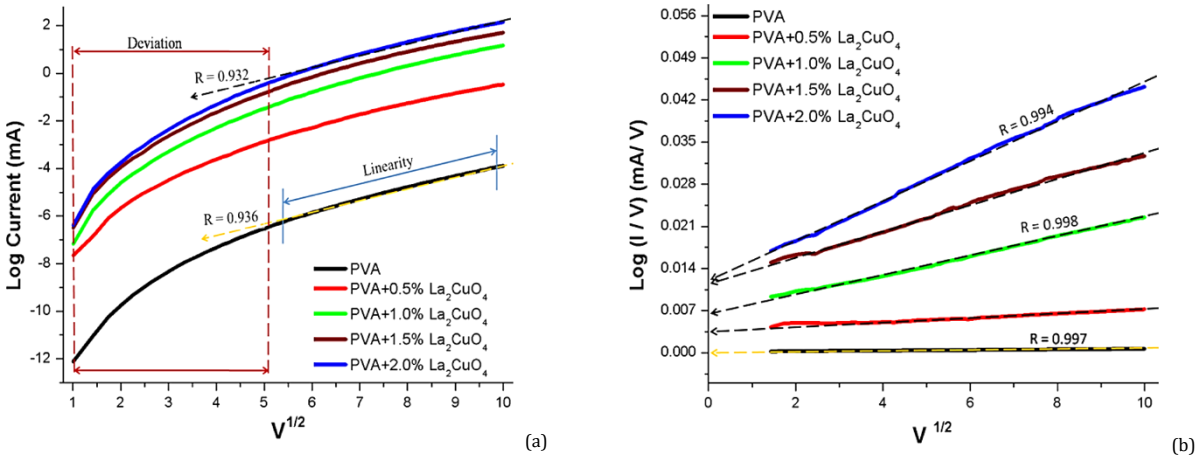

Figure 10. Plots of; a) Log (I) *versus* $V^{1/2}$ and b) Log (I/V) *versus* $V^{1/2}$ for PVA/La_2CuO_4 NCs at room temperature [82].

Physical interactions between the positive sites of the charge carriers and the polymeric matrix may have reduced the band-gap energy (E_g) of the composite films, and this led to an increase in *I*. Such phenomena of PNCs can be used to prepare electronic devices or sensors with a well-defined conductivity.

In addition, a significantly pronounced nonlinearity can be observed in the higher voltage region in Figure 9a, especially for NCs that contain 4-8 wt% of $CaAl_2ZnO_5$ NPs. The deviation or nonlinear characteristics in *I–V* curves can arise from a number of non-ohmic charge transport processes, such as space-charge limited conduction (SCLC), Schottky, and the Poole-Frenkel effect.

In the SCLC mechanism, the injected carriers are larger than the intrinsic carriers present in the film, creating a space-charge region near the interface and responsible for the bulk limited (SCLC) [112]. In the Schottky mechanism, the current is due to the transition of electrons between the cathode (metal electrode) and the NC film. In Poole-Frenkel mechanism, the emission of charge carriers trapped in the defect centers contributes to the conduction process [113], hence, it is a bulk limited process. To determine the exact mechanism responsible for the nonlinear variation of current with voltage, a detailed analysis of the *I-V* characteristics has been carried out.

In order to determine the exact mechanism of the charge transport in PVA-NC films, Saini *et al*. [114], Uma *et al*. [115], and Murad *et al*. [82], *etc*., reported a detailed analysis of the *I-V* characteristics has been carried out. For the SCLC mechanism, the *I-V* characteristic was plotted on a log-log scale (Figure 9b). To obtain the SCLC mechanism, the slope should be > 2 [116]. Figure 9b shows that the slopes of the graphs are < 2 and have values between 1.18 for pure PVA and 1.59 for NCs. Hence, SCLC is ruled out. Furthermore, to determine the conduction mechanism for PVA/La_2CuO_4 NCs, the linear fittings of the log current versus $V^{1/2}$ for Schottky emission and the log (I/V) versus $V^{1/2}$ for the Poole-Frenkel effect were plotted in Figures 10a and 10b, respectively.

Figure 10a for the Schottky mechanism shows that the graphs are nonlinear at lower voltage (< 5V) and only linear fitting in the higher voltage region, which exhibits the correlation coefficient (R) for the straight line is 0.93 as compared to the graphs obtained from the Poole-Frenkel mechanism where R is around 0.99 (Figure 10b). Thus, the Poole-Frenkel mechanism is the most appropriate responsible for the substantial increase in the conductivity of PVA/La_2CuO_4 NCs, with a lesser probability of Schottky emission, may be at higher voltages. There is a transition of the conduction mechanism from Poole-Frenkel to Schottky in the higher voltage regions at room temperature. However, El-Sayed *et al*. [117], demonstrated that the current–voltage (*I–V*) characteristics of the PVA/CMC-CuO NCs have nonohmic behaviour at higher voltages. The conduction mechanism in the PVA/CMC blend is Schottky emission at low temperature, whereas the Poole–Frenkel effect plays an important role in CuO-doped films at high temperatures.

Meanwhile, the experimental constant parameter, β_{exp} which is a characteristic of the conduction mechanism, can be estimated from the slope of the plots between log *I* and $V^{1/2}$ as shown in Figure 10a and Equation (1) as;

$$I\ \alpha\ exp\ = \left(\frac{e\ \beta\ V^{1/2}}{K\ T\ d^{1/2}}\right)\ ;\ \beta_{exp}\ = \left(\frac{m\ K\ T\ d^{1/2}}{e}\right) \quad (3)$$

Where, m is the slope of the plot, d is the thickness of the films, e is the electronic charge, T is the absolute temperature, and K is the Boltzmann constant. While the constant parameters of the Schottky emission, β_S and Poole-Frenkel emission, β_{PF} can be calculated as follows;

$$\beta_S\ = \left(\frac{e}{4\pi\ \varepsilon_s\ \varepsilon_0}\right)^{1/2}\ ;\ \beta_{PF}\ =\ 2\ \beta_S \quad (4)$$

Where ε_s is the dielectric constant of the films at higher frequency and ε_o is the permittivity of the free space (8.85×10^{-12} F/m). For NCs based on PVA/2wt% La_2CuO_4 [82], the estimated values of constant parameters β_{exp}, β_S and β_{PF} was 7.74×10^{-5}, 0.57×10^{-5} and 1.01×10^{-5} eV $V^{-1/2}$ $m^{1/2}$, respectively. The calculated β_{exp} values are closer to the values obtained from Poole–Frenkel (β_{PF}) method than the Schottky (β_s) method; hence, the Poole-Frenkel effect dominates the conduction mechanism in the PVA/La_2CuO_4 NC films. It may refer to a significant number of traps or defects created in the PVA structure after incorporation of La_2CuO_4 NPs. Similar results for PMMA-NCs were reported elsewhere by Goyal *et al*. [118].

According to the previous discussion, all optical and electrical parameters depend on the NP content and the range of interactions between NP-polymers at interfaces, so the ability of polymeric materials to modify its properties, such as the optical and electrical conductivity of NC films, provides utility in widening its use. Nanotechnology is an integral part of advanced hardware design for optoelectronic applications. The dimensional scale of electronic devices has now entered the nanorange. Therefore, the benefit of polymer-based NCs in these fields is quite diverse, includes many potential applications, and has been suggested for use in various applications such as Polymeric NCs that are promising materials for potential applications in electroluminescent, chemical sensors, electro catalysis, batteries, smart windows, and memory devices.

i. Polymeric NCs offer the promise of a new generation of hybrid materials with numerous applications, such as optical displays, catalysis, gas sensors, electrical, and photoconductor devices [119,120]. In addition to electroluminescent chemical sensors, electro catalysis, batteries, smart windows, and memory devices [121].
ii. Another potential application involves photovoltaic cells (PV), printable conductors, light-emitting diodes (LEDs), super capacitors, and field-effect transistors [122].
iii. Polymer-based solar cells have the ability to be used to make cheap, large flexible panels. The only downside is substantially low efficiency compared to commercial solar cells [123].
iv. PNCs based on conducting polymers with various nanometal oxides employed as nanowires have been evaluated for sensor applications including gas sensors, chemical sensors, and biosensors [124].

6. Conclusion

The progress in polymer nanocomposite materials properties has allowed numerous industrial utilizations in different multilevel applications in physical, chemical, biological, *etc*. Herein, a selection of representative and recent literature on different polymer nanocomposites was reviewed to highlight some of the issues related to the preparation, modification of the optical band gap, refractive indices, and AC-DC conductivity behaviour of the composites. As an illustration, the polymer nanocomposites are superior to the pure polymer matrix, and the effects of the nanometal oxides on the properties of the polymeric matrix are dependent upon many variables but especially upon the interaction between the nanometal oxides and the matrix. This review summarises that polymer nanocomposite materials have excellent potential for optoelectronic applications, because they offer unique features and properties.

Disclosure statement

Conflict of interests: The authors declare that they have no conflict of interest.
Ethical approval: All ethical guidelines have been adhered.

CRediT authorship contribution statement

Conceptualization: Murad Qassim Abdulraqeb Al-Gunaid, Fares Hezam Al-Ostoot; Methodology: Murad Qassim Abdulraqeb Al-Gunaid, Gayitri Hebbur Maheshwarappa; Software: Shashikala Badaga Shivanna, Mohammed Ali Hussein Dhaif-Allah; Validation: Murad Qassim Abdulraqeb Al-Gunaid, Waled Abdo Ahmed; Formal Analysis: Fares Hezam Al-Ostoot, Murad Qassim Abdulraqeb Al-Gunaid; Investigation: Murad Qassim Abdulraqeb Al-Gunaid, Waled Abdo Ahmed; Resources: Fares Hezam Al-Ostoot, Mohammed Ali Hussein Dhaif-Allah; Data Curation: Murad Qassim Abdulraqeb Al-Gunaid, Gayitri Hebbur Maheshwarappa; Writing - Original Draft: Murad Qassim Abdulraqeb Al-Gunaid, Fares Hezam Al-Ostoot; Writing - Review and Editing: Fares Hezam Al-Ostoot, Shashikala Badaga Shivanna; Visualization: Murad Qassim Abdulraqeb Al-Gunaid, Fares Hezam Al-Ostoot; Supervision: Murad Qassim Abdulraqeb Al-Gunaid, Fares Hezam Al-Ostoot; Project Administration: Fares Hezam Al-Ostoot, Murad Qassim Abdulraqeb Al-Gunaid.

ORCID and Email

Murad Qassim Abdulraqeb Al-Gunaid
morad.jounid11@gmail.com
muradal-gunaid@tu.edu.ye
https://orcid.org/0000-0001-5071-6128
Gayitri Hebbur Maheshwarappa
gayitrikumar@sjce.ac.in
https://orcid.org/0000-0003-2653-9883
Shashikala Badaga Shivanna
shashisuni30@gmail.com
https://orcid.org/0000-0001-9049-8882
Mohammed Ali Hussein Dhaif-Allah
mdhaif2014@gmail.com
https://orcid.org/0000-0002-9878-5840
Waled Abdo Ahmed
waled.abdulrab@tu.edu.ye
https://orcid.org/0000-0001-8185-833X
Fares Hezam Al-Ostoot
faresalostoot@gmail.com
faresalostoot@baydaauniv.net
https://orcid.org/0000-0003-4571-6419

References

[1]. Feng, C.; Kou, X.; Chen, B.; Qian, G.; Sun, Y.; Lu, G. One-pot synthesis of In doped NiO nanofibers and their gas sensing properties. *Sens. Actuators B Chem.* **2017**, *253*, 584–591.
[2]. Wei, Y.; Wang, X.; Yi, G.; Zhou, L.; Cao, J.; Sun, G.; Chen, Z.; Bala, H.; Zhang, Z. Hydrothermal synthesis of Ag modified ZnO nanorods and their enhanced ethanol-sensing properties. *Mater. Sci. Semicond. Process.* **2018**, *75*, 327–333.
[3]. Mühlberg, M. Retraction: Recent advances of metal–metal oxide nanocomposites and their tailored nanostructures in numerous catalytic applications. *J. Mater. Chem. A Mater. Energy Sustain.* **2020**, *8*, 15189–15189.
[4]. Goswami, C.; Hazarika, K. K.; Bharali, P. Transition metal oxide nanocatalysts for oxygen reduction reaction. *Mater. Sci. Energy Technol.* **2018**, *1*, 117–128.
[5]. Leng, Y.; Guo, W.; Shi, X.; Li, Y.; Xing, L. Polyhydroquinone-coated Fe3O4 nanocatalyst for degradation of rhodamine B based on sulfate radicals. *Ind. Eng. Chem. Res.* **2013**, *52*, 13607–13612.
[6]. Hu, Z.; Wu, Z.; Han, C.; He, J.; Ni, Z.; Chen, W. Two-dimensional transition metal dichalcogenides: interface and defect engineering. *Chem. Soc. Rev.* **2018**, *47*, 3100–3128.

[7]. Kumar, P.; Rawat, N.; Hang, D.-R.; Lee, H.-N.; Kumar, R. Controlling band gap and refractive index in dopant-free α-Fe2O3 films. *Electron. Mater. Lett.* **2015**, *11*, 13–23.

[8]. Goh, E. G.; Xu, X.; McCormick, P. G. Effect of particle size on the UV absorbance of zinc oxide nanoparticles. *Scr. Mater.* **2014**, *78–79*, 49–52.

[9]. Ali, A.; Rahman, G.; Ali, T.; Nadeem, M.; Hasanain, S. K.; Sultan, M. Enhanced band edge luminescence of ZnO nanorods after surface passivation with ZnS. *Physica E Low Dimens. Syst. Nanostruct.* **2018**, *103*, 329–337.

[10]. Camargo, P. H. C.; Satyanarayana, K. G.; Wypych, F. Nanocomposites: synthesis, structure, properties and new application opportunities. *Mater. Res.* **2009**, *12*, 1–39.

[11]. Saeed, A. M. N.; Al-Gunaid, M. Q. A.; Siddaramaiah Effect of lithium perchlorate on the optoelectrical and thermal properties of poly(vinylpyrrolidone)/nano-cesium aluminate solid polymer electrolytes. *Polym. Plast. Technol. Eng.* **2018**, *57*, 1554–1566.

[12]. Alkanad, K.; Hezam, A.; Sujay Shekar, G. C.; Drmosh, Q. A.; Amrutha Kala, A. L.; AL-Gunaid, M. Q. A.; Lokanath, N. K. Magnetic recyclable α-Fe2O3–Fe3O4/Co3O4–CoO nanocomposite with a dual Z-scheme charge transfer pathway for quick photo-Fenton degradation of organic pollutants. *Catal. Sci. Technol.* **2021**, *11*, 3084–3097.

[13]. Liu, X.; Jiang, Z.; Li, J.; Zhang, Z.; Ren, L. Super-hydrophobic property of nano-sized cupric oxide films. *Surf. Coat. Technol.* **2010**, *204*, 3200–3204.

[14]. Liu, X.; Iocozzia, J.; Wang, Y.; Cui, X.; Chen, Y.; Zhao, S.; Li, Z.; Lin, Z. Noble metal–metal oxide nanohybrids with tailored nanostructures for efficient solar energy conversion, photocatalysis and environmental remediation. *Energy Environ. Sci.* **2017**, *10*, 402–434.

[15]. Toroker, M. C.; Carter, E. A. Transition metal oxide alloys as potential solar energy conversion materials. *J. Mater. Chem. A Mater. Energy Sustain.* **2013**, *1*, 2474–2484.

[16]. Lany, S. Semiconducting transition metal oxides. *J. Phys. Condens. Matter* **2015**, *27*, 283203.

[17]. Elilarassi, R.; Chandrasekaran, G. Structural, optical and magnetic characterization of Cu-doped ZnO nanoparticles synthesized using solid state reaction method. *J. Mater. Sci.: Mater. Electron.* **2010**, *21*, 1168–1173.

[18]. Cho, S.; Jung, S.-H.; Lee, K.-H. Morphology-controlled growth of ZnO nanostructures using microwave irradiation: From basic to complex structures. *J. Phys. Chem. C Nanomater. Interfaces* **2008**, *112*, 12769–12776.

[19]. Janotti, A.; Van de Walle, C. G. Fundamentals of zinc oxide as a semiconductor. *Rep. Prog. Phys.* **2009**, *72*, 126501.

[20]. Look, D. C.; Leedy, K. D.; Vines, L.; Svensson, B. G.; Zubiaga, A.; Tuomisto, F.; Doutt, D. R.; Brillson, L. J. Self-compensation in semiconductors: The Zn vacancy in Ga-doped ZnO. *Phys. Rev. B* **2011**, *84*, 115202.

[21]. Puchala, B.; Morgan, D. Publisher's Note: Stable interstitial dopant–vacancy complexes in ZnO [Phys. Rev. B 85, 195207 (2012)]. *Phys. Rev. B Condens. Matter Mater. Phys.* **2013**, *87*, 079908.

[22]. Baek, S.-D.; Biswas, P.; Kim, J.-W.; Kim, Y. C.; Lee, T. I.; Myoung, J.-M. Low-temperature facile synthesis of Sb-doped p-type ZnO nanodisks and its application in homojunction light-emitting diode. *ACS Appl. Mater. Interfaces* **2016**, *8*, 13018–13026.

[23]. Han, N. S.; Shim, H. S.; Seo, J. H.; Kim, S. Y.; Park, S. M.; Song, J. K. Defect states of ZnO nanoparticles: Discrimination by time-resolved photoluminescence spectroscopy. *J. Appl. Phys.* **2010**, *107*, 084306.

[24]. Borysiewicz, M. A. ZnO as a functional material, a review. *Crystals (Basel)* **2019**, *9*, 505.

[25]. Alvi, N. H.; ul Hasan, K.; Nur, O.; Willander, M. The origin of the red emission in n-ZnO nanotubes/p-GaN white light emitting diodes. *Nanoscale Res. Lett.* **2011**, *6*, 130.

[26]. Lee, Y.-S.; Gopi, C. V. V. M.; Eswar Reddy, A.; Nagaraju, C.; Kim, H.-J. High performance of TiO2/CdS quantum dot sensitized solar cells with a Cu–ZnS passivation layer. *New J Chem* **2017**, *41*, 1914–1917.

[27]. Devan, R. S.; Patil, R. A.; Lin, J.-H.; Ma, Y.-R. One-dimensional metal-oxide nanostructures: Recent developments in synthesis, characterization, and applications. *Adv. Funct. Mater.* **2012**, *22*, 3326–3370.

[28]. Scotti, N.; Monticelli, D.; Zaccheria, F. Dispersed copper oxide: A multifaceted tool in catalysis. *Inorganica Chim. Acta* **2012**, *380*, 194–200.

[29]. Hassan, M. S.; Amna, T.; Yang, O.-B.; El-Newehy, M. H.; Al-Deyab, S. S.; Khil, M.-S. Smart copper oxide nanocrystals: synthesis, characterization, electrochemical and potent antibacterial activity. *Colloids Surf. B Biointerfaces* **2012**, *97*, 201–206.

[30]. Navidpour, A. H.; Abbasi, S.; Li, D.; Mojiri, A.; Zhou, J. L. Investigation of advanced oxidation process in the presence of TiO2 semiconductor as photocatalyst: Property, principle, kinetic analysis, and photocatalytic activity. *Catalysts* **2023**, *13*, 232.

[31]. Singh, M. K.; Mehata, M. S. Phase-dependent optical and photocatalytic performance of synthesized titanium dioxide (TiO2) nanoparticles. *Optik (Stuttg.)* **2019**, *193*, 163011.

[32]. Motoyoshi, R.; Oku, T.; Kidowaki, H.; Suzuki, A.; Kikuchi, K.; Kikuchi, S.; Jeyadevan, B. Structure and photovoltaic activity of cupric oxide-based thin film solar cells. *J. Ceram. Soc. Japan* **2010**, *118*, 1021–1023.

[33]. Moura, A. P.; Cavalcante, L. S.; Sczancoski, J. C.; Stroppa, D. G.; Paris, E. C.; Ramirez, A. J.; Varela, J. A.; Longo, E. Structure and growth mechanism of CuO plates obtained by microwave-hydrothermal without surfactants. *Adv. Powder Technol.* **2010**, *21*, 197–202.

[34]. Gao, L.; Pang, C.; He, D.; Shen, L.; Gupta, A.; Bao, N. Synthesis of hierarchical nanoporous microstructures via the Kirkendall effect in chemical reduction process. *Sci. Rep.* **2015**, *5*, 16061.

[35]. Farghali, A. A.; Bahgat, M.; Enaiet Allah, A.; Khedr, M. H. Adsorption of Pb(II) ions from aqueous solutions using copper oxide nanostructures. *Beni-Suef Univ. J. Basic Appl. Sci.* **2013**, *2*, 61–71.

[36]. Yecheskel, Y.; Dror, I.; Berkowitz, B. Catalytic degradation of brominated flame retardants by copper oxide nanoparticles. *Chemosphere* **2013**, *93*, 172–177.

[37]. Aslani, A.; Oroojpour, V. CO gas sensing of CuO nanostructures, synthesized by an assisted solvothermal wet chemical route. *Physica B Condens. Matter* **2011**, *406*, 144–149.

[38]. Xu, J. F.; Ji, W.; Shen, Z. X.; Li, W. S.; Tang, S. H.; Ye, X. R.; Jia, D. Z.; Xin, X. Q. Raman spectra of CuO nanocrystals. *J. Raman Spectrosc.* **1999**, *30*, 413–415.

[39]. Wang, W.; Zhou, Q.; Fei, X.; He, Y.; Zhang, P.; Zhang, G.; Peng, L.; Xie, W. Synthesis of CuO nano- and micro-structures and their Raman spectroscopic studies. *CrystEngComm* **2010**, *12*, 2232–2237.

[40]. Wu, D.; Zhang, Q.; Tao, M. LSDA+Ustudy of cupric oxide: Electronic structure and native point defects. *Phys. Rev. B Condens. Matter Mater. Phys.* **2006**, *73*, 235206.

[41]. Mallick, G.; Labh, J.; Giri, L.; Pandey, A. C.; Karna, S. P. Facile synthesis and electron transport properties of NiO nanostructures investigated by scanning tunneling microscopy. *AIP Adv.* **2017**, *7*, 085007.

[42]. Shang, S.; Xue, K.; Chen, D.; Jiao, X. Preparation and characterization of rose-like NiO nanostructures. *CrystEngComm* **2011**, *13*, 5094–5099.

[43]. Dubal, D. P.; Gomez-Romero, P.; Sankapal, B. R.; Holze, R. Nickel cobaltite as an emerging material for supercapacitors: An overview. *Nano Energy* **2015**, *11*, 377–399.

[44]. El-Kemary, M.; Nagy, N.; El-Mehasseb, I. Nickel oxide nanoparticles: Synthesis and spectral studies of interactions with glucose. *Mater. Sci. Semicond. Process.* **2013**, *16*, 1747–1752.

[45]. Abbasi, M. A.; Ibupoto, Z. H.; Hussain, M.; Khan, Y.; Khan, A.; Nur, O.; Willander, M. Potentiometric zinc ion sensor based on honeycomb-like NiO nanostructures. *Sensors (Basel)* **2012**, *12*, 15424–15437.

[46]. He, T.; Yao, J. Photochromic materials based on tungsten oxide. *J. Mater. Chem.* **2007**, *17*, 4547–4557.

[47]. Gu, Z.; Ma, Y.; Yang, W.; Zhang, G.; Yao, J. Self-assembly of highly oriented one-dimensional h-WO3 nanostructures. *Chem. Commun. (Camb.)* **2005**, 3597–3599.

[48]. Polleux, J.; Pinna, N.; Antonietti, M.; Niederberger, M. Growth and assembly of crystalline tungsten oxide nanostructures assisted by bioligation. *J. Am. Chem. Soc.* **2005**, *127*, 15595–15601.

[49]. Zhao, Z.-G.; Miyauchi, M. Nanoporous-walled tungsten oxide nanotubes as highly active visible-light-driven photocatalysts. *Angew. Chem. Int. Ed Engl.* **2008**, *47*, 7051–7055.

[50]. Zhao, Z.-G.; Miyauchi, M. Shape modulation of tungstic acid and tungsten oxide hollow structures. *J. Phys. Chem. C Nanomater. Interfaces* **2009**, *113*, 6539–6546.

[51]. Chatterjee, A. Properties improvement of PMMA using nano TiO2. *J. Appl. Polym. Sci.* **2010**, *118*, 2890–2897.

[52]. Kruenate, J.; Tongpool, R.; Panyathanmaporn, T.; Kongrat, P. Optical and mechanical properties of polypropylene modified by metal oxides. *Surf. Interface Anal.* **2004**, *36*, 1044–1047.

[53]. Khanmohammadi, S.; Babazadeh, M. Synthesis of polythiophene/manganese dioxide nanocomposites by in-situ core-shell polymerization method and study of their physical properties. *J. Nanostructures* **2018**, *8*, 366–373.

[54]. Mittal, V. Polymer Layered Silicate Nanocomposites: A Review. *Materials (Basel)* **2009**, *2*, 992–1057.

[55]. Yasmeen, S.; Iqbal, F.; Munawar, T.; Nawaz, M. A.; Asghar, M.; Hussain, A. Synthesis, structural and optical analysis of surfactant assisted ZnO–NiO nanocomposites prepared by homogeneous precipitation method. *Ceram. Int.* **2019**, *45*, 17859–17873.

[56]. Al-Gunaid, M. Q. A.; Saeed, A. M. N.; Siddaramaiah Effects of the electrolyte content on the electrical permittivity, thermal stability, and optical dispersion of poly(vinyl alcohol)-cesium copper oxide-lithium perchlorate nanocomposite solid-polymer electrolytes. *J. Appl. Polym. Sci.* **2018**, *135*, 45852.

[57]. Al-Gunaid, M. Q. A.; Shashikala, B. S.; Gayitri, H. M.; Alkanad, K.; Al-Zaqri, N.; Boshaala, A.; Al-Ostoot, F. H. Characterization of opto-electrical, electrochemical and mechanical behaviors of flexible PVA/(PANI+La2CuO4)/LiClO4-PC polymer blend electrolyte films. *Macromol. Res.* **2022**, *30*, 650–658.

[58]. Du, J.-H.; Bai, J.; Cheng, H.-M. The present status and key problems of carbon nanotube based polymer composites. *EXPRESS Polym. Lett.* **2007**, *1*, 253–273.

[59]. Alateyah, A. I.; Dhakal, H. N.; Zhang, Z. Y. Processing, properties, and applications of polymer nanocomposites based on layer silicates: A review. *Adv. Polym. Technol.* **2013**, *32*.
[60]. Ghezelbash, Z.; Ashouri, D.; Mousavian, S.; Ghandi, A. H.; Rahnama, Y. Surface modified AlO in fluorinated polyimide/AlO nanocomposites: Synthesis and characterization. *Bull. Mater. Sci.* **2012**, *35*, 925–931.
[61]. Althues, H.; Henle, J.; Kaskel, S. Functional inorganic nanofillers for transparent polymers. *Chem. Soc. Rev.* **2007**, *36*, 1454–1465.
[62]. Fujita, M.; Idota, N.; Matsukawa, K.; Sugahara, Y. Preparation of oleyl phosphate-modified TiO2/poly(methyl methacrylate) hybrid thin films for investigation of their optical properties. *J. Nanomater.* **2015**, *2015*, 1–7.
[63]. Mallakpour, S.; Madani, M. Use of silane coupling agent for surface modification of zinc oxide as inorganic filler and preparation of poly(amide-imide)/zinc oxide nanocomposite containing phenylalanine moieties. *Bull. Mater. Sci. (India)* **2012**, *35*, 333–339.
[64]. Aminuzzaman, M.; Mitsuishi, M.; Miyashita, T. Surface modification of a flexible polyimide film using a reactive fluorinated polymer nanosheet. *Thin Solid Films* **2010**, *519*, 974–977.
[65]. Babicheva, V. E.; Boltasseva, A.; Lavrinenko, A. V. Transparent conducting oxides for electro-optical plasmonic modulators. *Nanophotonics* **2015**, *4*, 165–185.
[66]. Dorranian, D.; Golian, Y.; Hojabri, A. Investigation of nitrogen plasma effect on the nonlinear optical properties of PMMA. *J. Theor. Appl. Phys.* **2012**, *6*, 1.
[67]. Al-Ammar, K.; Hashim, A.; Husaien, M. Synthesis and study of optical properties of (PMMA-CrCl2) composites. *Chem. Mater. Eng.* **2013**, *1*, 85–87.
[68]. Mustafa, F. A. Optical properties of NaI doped polyvinyl alcohol films. *Physical Sciences Research International* **2013**, *1*, 1–9.
[69]. Quadri, T. W.; Olasunkanmi, L. O.; Fayemi, O. E.; Solomon, M. M.; Ebenso, E. E. Zinc oxide nanocomposites of selected polymers: Synthesis, characterization, and corrosion inhibition studies on mild steel in HCl solution. *ACS Omega* **2017**, *2*, 8421–8437.
[70]. Shanshool, H. M.; Yahaya, M.; Yunus, W. M. M.; Abdullah, I. Y. Investigation of energy band gap in polymer/ZnO nanocomposites. *J. Mater. Sci.: Mater. Electron.* **2016**, *27*, 9804–9811.
[71]. Cao, H. Q.; Qiu, X. Q.; Luo, B.; Liang, Y.; Zhang, Y. H.; Tan, R. Q.; Zhao, M. J.; Zhu, Q. M. Synthesis and room-temperature ultraviolet photoluminescence properties of Zirconia nanowires. *Adv. Funct. Mater.* **2004**, *14*, 243–246.
[72]. Mallakpour, S.; Shafiee, E. The synthesis of poly(vinyl chloride) nanocomposite films containing ZrO2 nanoparticles modified with vitamin B1 with the aim of improving the mechanical, thermal and optical properties. *Des. Monomers Polym.* **2017**, *20*, 378–388.
[73]. Mallakpour, S.; Hajjari, Z. Ultrasound-assisted surface treatment of ZrO2 with BSA and incorporating in PVC to improve the properties of the obtained nanocomposites: Fabrication and characterization. *Ultrason. Sonochem.* **2018**, *41*, 350–360.
[74]. Taha, T. A.; Hendawy, N.; El-Rabaie, S.; Esmat, A.; El-Mansy, M. K. Effect of NiO NPs doping on the structure and optical properties of PVC polymer films. *Polym. Bull. (Berl.)* **2019**, *76*, 4769–4784.
[75]. Shivanna, S. B.; Al-Gunaid, M. Q. A.; Al-Ostoot, F. H.; Al-Zaqri, N.; Boshaala, A.; Siddaramaiah; Anasuya, S. J. Probing optical efficiency and electrochemical behaviors of polycarbonate incorporating conducting PANI and halloysite nanotubes (HNTs) as core–shell nanofillers. *Polym. Bull. (Berl.)* **2022**, *79*, 10333–10355.
[76]. Hanumaiah Anupama, B.; AL-Gunaid, M. Q. A.; Shivanna Shasikala, B.; Theranya Ereppa, S.; Kavya, R.; Hatna Siddaramaiah, B.; Sangameshwara Madhukar, B. Poly (o-anisidine) encapsulated K 2 ZrO 3 nano-core based gelatin nano composites: Investigations of optical, thermal, microcrystalline and morphological characteristics. *ChemistrySelect* **2022**, *7*, e202201621.
[77]. Al-Hakimi, A. N.; Asnag, G. M.; Alminderej, F.; Alhagri, I. A.; Al-Hazmy, S. M.; Qahtan, T. F. Enhancing the structural, optical, thermal, and electrical properties of PVA filled with mixed nanoparticles (TiO2/Cu). *Crystals (Basel)* **2023**, *13*, 135.
[78]. Duchaniya, R. K.; Choudhary, N. Synthesis and characterization of PVA/TiO2 nanocomposite . *Key Eng. Mater.* **2017**, *737*, 242–247.
[79]. Li, Y.; Zhang, Z.; Zhu, J. Broadband optical limiting properties of Tungsten Trioxide-Poly (Vinyl Alcohol) solid-state nanocomposite films. *Opt. Mater. (Amst.)* **2021**, *119*, 111359.
[80]. Selvi, J.; Mahalakshmi, S.; Parthasarathy, V.; Hu, C.; Lin, Y.-F.; Tung, K.-L.; Anbarasan, R.; Annie, A. A. Optical, thermal, mechanical properties, and non-isothermal degradation kinetic studies on PVA/CuO nanocomposites. *Polym. Compos.* **2019**, *40*, 3737–3748.
[81]. Abdullah, O. G.; Aziz, S. B.; Omer, K. M.; Salih, Y. M. Reducing the optical band gap of polyvinyl alcohol (PVA) based nanocomposite. *J. Mater. Sci.: Mater. Electron.* **2015**, *26*, 5303–5309.
[82]. Al-Gunaid, M. Q. A.; Saeed, A. M. N.; Gayitri; Basavarajaiah, S. Impact of nano-perovskite La2CuO4 on dc-conduction, opto-electrical sensing and thermal behavior of PVA nanocomposite films. *Polymer-Plastics Technology and Materials* **2020**, *59*, 469–483.
[83]. Somesh, T. E.; Al-Gunaid, M. Q. A.; Madhukar, B. S.; Siddaramaiah Photosensitization of optical band gap modified polyvinyl alcohol films with hybrid AgAlO2 nanoparticles. *J. Mater. Sci.: Mater. Electron.* **2019**, *30*, 37–49.
[84]. Gayitri; Al-Gunaid, M.; Madhukar; Siddaramaiah, B.; Prakash, G. Structural, dielectric permittivity and optical characteristics of casting poly vinyl alcohol/calcium nickel aluminate nanocomposite films. *Polymer-Plastics Technology and Materials* **2019**, *58*, 1110–1124.
[85]. Ung, B.; Dupuis, A.; Stoeffler, K.; Dubois, C.; Skorobogatiy, M. High-refractive-index composite materials for terahertz waveguides: trade-off between index contrast and absorption loss. *J. Opt. Soc. Am. B* **2011**, *28*, 917–921.
[86]. Al-Gunaid, M. Q. A.; Saeed, A. M. N.; Subramani, N. K.; Madhukar, B. S.; Siddaramaiah Optical parameters, electrical permittivity and I–V characteristics of PVA/Cs2CuO2 nanocomposite films for opto-electronic applications. *J. Mater. Sci.: Mater. Electron.* **2017**, *28*, 8074–8086.
[87]. Mahendia, S.; Kumar Tomar, A.; Goyal, P. K.; Kumar, S. Tuning of refractive index of poly(vinyl alcohol): Effect of embedding Cu and Ag nanoparticles. *J. Appl. Phys.* **2013**, *113*, 073103.
[88]. An, N.; Zhuang, B.; Li, M.; Lu, Y.; Wang, Z.-G. Combined theoretical and experimental study of refractive indices of water-acetonitrile-salt systems. *J. Phys. Chem. B* **2015**, *119*, 10701–10709.
[89]. Al-Gunaid, M. Q. A.; Somesh; Gayitri; Al-Ostoot, F. H.; Basavarajaiah, S. Optimized nano-perovskite lanthanum cuprate decorated PVA based solid polymer electrolyte. *Polymer-Plastics Technology and Materials* **2020**, *59*, 215–229.
[90]. Wang, Z.; Lu, Z.; Mahoney, C.; Yan, J.; Ferebee, R.; Luo, D.; Matyjaszewski, K.; Bockstaller, M. R. Transparent and high refractive index thermoplastic polymer glasses using evaporative ligand exchange of hybrid particle fillers. *ACS Appl. Mater. Interfaces* **2017**, *9*, 7515–7522.
[91]. Yuwono, A. H.; Liu, B.; Xue, J.; Wang, J.; Elim, H. I.; Ji, W.; Li, Y.; White, T. J. Controlling the crystallinity and nonlinear optical properties of transparent TiO2–PMMA nanohybrids. *J. Mater. Chem.* **2004**, *14*, 2978–2987.
[92]. Takahashi, S.; Hotta, S.; Watanabe, A.; Idota, N.; Matsukawa, K.; Sugahara, Y. Modification of TiO2 nanoparticles with oleyl phosphate via phase transfer in the toluene–water system and application of modified nanoparticles to cyclo-olefin-polymer-based organic–inorganic hybrid films exhibiting high refractive indices. *ACS Appl. Mater. Interfaces* **2017**, *9*, 1907–1912.
[93]. Tsai, C.-M.; Hsu, S.-H.; Ho, C.-C.; Tu, Y.-C.; Tsai, H.-C.; Wang, C.-A.; Su, W.-F. High refractive index transparent nanocomposites prepared by in situ polymerization. *J. Mater. Chem. C Mater. Opt. Electron. Devices* **2014**, *2*, 2251–2258.
[94]. Dan, S.; Gu, H.; Tan, J.; Zhang, B.; Zhang, Q. Transparent epoxy/TiO2 optical hybrid films with tunable refractive index prepared via a simple and efficient way. *Prog. Org. Coat.* **2018**, *120*, 252–259.
[95]. Saeed, A. M. N.; Al-Gunaid, M. Q. A.; Subramani, N. K.; Madhukar; Basavarajaiah, S. Effect of cesium aluminate nanofiller on optical properties of polyvinyl pyrrolidone nanocomposite films. *Polym. Plast. Technol. Eng.* **2018**, *57*, 1188–1196.
[96]. Choudhary, S.; Sengwa, R. J. ZnO nanoparticles dispersed PVA–PVP blend matrix based high performance flexible nanodielectrics for multifunctional microelectronic devices. *Curr. Appl. Phys.* **2018**, *18*, 1041–1058.
[97]. Liu, C.; Hajagos, T. J.; Chen, D.; Chen, Y.; Kishpaugh, D.; Pei, Q. Efficient one-pot synthesis of colloidal zirconium oxide nanoparticles for high-refractive-index nanocomposites. *ACS Appl. Mater. Interfaces* **2016**, *8*, 4795–4802.
[98]. Shashikala; Al-Gunaid, M. Q. A.; Anupama; Anasuya; Siddaramaiah Tailoring structural, opto-electrical and electrochemical properties of PC impregnated core-shell (PANI-NaBiO2) nanocomposites. *Polymer-Plastics Technology and Materials* **2021**, *60*, 1656–1671.
[99]. Bommalapura Hanumaiah, A.; Al-Gunaid, M. Q. A.; Siddaramaiah Performance of nano-K-doped zirconate on modified opto-electrical and electrochemical properties of gelatin biopolymer nanocomposites. *Polym. Bull. (Berl.)* **2021**, *78*, 3023–3041.
[100]. Xia, Y.; Zhang, C.; Wang, J.-X.; Wang, D.; Zeng, X.-F.; Chen, J.-F. Synthesis of transparent aqueous ZrO2 nanodispersion with a controllable crystalline phase without modification for a high-refractive-index nanocomposite film. *Langmuir* **2018**, *34*, 6806–6813.
[101]. Gayitri, H. M.; Al-Gunaid, M. Q. A.; AL-Ostoot, F. H.; Al-Zaqri, N.; Boshaala, A.; Gnanaprakash, A. P. Investigation on opto-electrical, structural and electro-chemical performance of PVA/ZnBi2MoO7 hybrid nanocomposites. *Polym. Bull. (Berl.)* **2023**, *80*, 773–790.
[102]. Ma, C.-C. M.; Chen, Y.-J.; Kuan, H.-C. Polystyrene nanocomposite materials—Preparation, mechanical, electrical and thermal properties, and morphology. *J. Appl. Polym. Sci.* **2006**, *100*, 508–515.
[103]. Maji, P.; Choudhary, R. B.; Majhi, M. Structural, electrical and optical properties of silane-modified ZnO reinforced PMMA matrix and its catalytic activities. *J. Non Cryst. Solids* **2017**, *456*, 40–48.
[104]. Morsi, M. A.; Abdelaziz, M.; Oraby, A. H.; Mokhles, I. Structural, optical, thermal, and dielectric properties of polyethylene oxide/ carboxymethyl cellulose blend filled with barium titanate. *J. Phys. Chem. Solids* **2019**, *125*, 103–114.

[105]. Rajesh; Crasta, V.; Kumar, R.; Shetty, G.; Sangappa, Y.; Kudva, J.; Vijeth Effect of MoO3 nanofiller on structural, optical, mechanical, dielectric and thermal properties of PVA/PVP blend. *Mater. Res. Innov.* **2020**, *24*, 270–278.
[106]. Chandrakala, H. N.; Ramaraj, B.; Shivakumaraiah; Siddaramaiah Optical properties and structural characteristics of zinc oxidecerium oxide doped polyvinyl alcohol films. *J. Alloys Compd.* **2014**, *586*, 333–342.
[107]. Suma, G. R.; Subramani, N. K.; Sachhidananda, S.; Satyanarayana, S. V.; Siddaramaiah Optical and electrical evaluation of Ag0.5Cu0.75O introduced poly(vinyl alcohol) based E.Coli sensors. *J. Mater. Sci.: Mater. Electron.* **2017**, *28*, 13139–13148.
[108]. Saeed, A. M. N.; Hezam, A.; Al-Gunaid, M. Q. A.; Somesh; Siddaramaiah Effect of ethylene carbonate on properties of PVP-CsAlO2-LiClO4 solid polymer electrolytes. *Polymer-Plastics Technology and Materials* **2021**, *60*, 132–146.
[109]. Saini, I.; Sharma, A.; Dhiman, R.; Aggarwal, S.; Ram, S.; Sharma, P. K. Grafted SiC nanocrystals: For enhanced optical, electrical and mechanical properties of polyvinyl alcohol. *J. Alloys Compd.* **2017**, *714*, 172–180.
[110]. Gayitri, H. M.; AL-Gunaid, M.; Siddaramaiah; Gnana Prakash, A. P. Investigation of triplex CaAl2ZnO5 nanocrystals on electrical permittivity, optical and structural characteristics of PVA nanocomposite films. *Polym. Bull. (Berl.)* **2020**, *77*, 5005–5026.
[111]. Rozra, J.; Saini, I.; Sharma, A.; Chandak, N.; Aggarwal, S.; Dhiman, R.; Sharma, P. K. Cu nanoparticles induced structural, optical and electrical modification in PVA. *Mater. Chem. Phys.* **2012**, *134*, 1121–1126.
[112]. Cheong, K. Y.; Moon, J. H.; Kim, H. J.; Bahng, W.; Kim, N.-K. Current conduction mechanisms in atomic-layer-deposited HfO2/nitrided SiO2 stacked gate on 4H silicon carbide. *J. Appl. Phys.* **2008**, *103*, 084113.
[113]. Mansour, S. A.; Al-Ghoury, M. E.; Shalaan, E.; El Eraki, M. H. I.; Abdel-Bary, E. M. Electrical properties and transport conduction mechanism of nitrile rubber/poly(vinyl chloride) blend. *J. Appl. Polym. Sci.* **2010**, *116*, 3134–3139.
[114]. Saini, I.; Rozra, J.; Chandak, N.; Aggarwal, S.; Sharma, P. K.; Sharma, A. Tailoring of electrical, optical and structural properties of PVA by addition of Ag nanoparticles. *Mater. Chem. Phys.* **2013**, *139*, 802–810.
[115]. Devi, C. U.; Sharma, A. K.; Rao, V. V. R. N. Electrical and optical properties of pure and silver nitrate-doped polyvinyl alcohol films. *Mater. Lett.* **2002**, *56*, 167–174.
[116]. Anjaneyulu, P.; Sangeeth, C. S. S.; Menon, R. Space-charge limited conduction in doped polypyrrole devices. *J. Appl. Phys.* **2010**, *107*, 093716.
[117]. El Sayed, A. M.; El-Gamal, S.; Morsi, W. M.; Mohammed, G. Effect of PVA and copper oxide nanoparticles on the structural, optical, and electrical properties of carboxymethyl cellulose films. *J. Mater. Sci.* **2015**, *50*, 4717–4728.
[118]. Goyal, A.; Sharma, A.; Saini, I.; Chandak, N.; Sharma, P. Tailoring of optical and electrical properties of PMMA by incorporation of Ag nanoparticles. *Bull. Mater. Sci. (India)* **2017**, *40*, 615–621.
[119]. Mir, S. H.; Nagahara, L. A.; Thundat, T.; Mokarian-Tabari, P.; Furukawa, H.; Khosla, A. Review—organic-inorganic hybrid functional materials: An integrated platform for applied technologies. *J. Electrochem. Soc.* **2018**, *165*, B3137–B3156.
[120]. Shashikala, B. S.; Al-Gunaid, M. Q. A.; Somesh, T. E.; Anasuya, S. J.; Siddaramaiah Core–shell synergistic effect of (PANI-NaBiO2) incorporated polycarbonate films to photodegradation of MG dye and photovoltaic activity. *Polym. Bull. (Berl.)* **2022**, *79*, 7531–7554.
[121]. Kausar, A. Potential of Polymer/Graphene Nanocomposite in Electronics. *American Journal of Nanoscience and Nanotechnology Research* **2018**, *6*, 1–9, https://core.ac.uk/download/pdf/286338353.pdf.
[122]. Baibarac, M.; Gómez-Romero, P. Nanocomposites based on conducting polymers and carbon nanotubes: from fancy materials to functional applications. *J. Nanosci. Nanotechnol.* **2006**, *6*, 289–302.
[123]. Mayer, A. C.; Scully, S. R.; Hardin, B. E.; Rowell, M. W.; McGehee, M. D. Polymer-based solar cells. *Mater. Today (Kidlington)* **2007**, *10*, 28–33.
[124]. Park, S. J.; Kwon, O. S.; Lee, J. E.; Jang, J.; Yoon, H. Conducting polymer-based nanohybrid transducers: a potential route to high sensitivity and selectivity sensors. *Sensors (Basel)* **2014**, *14*, 3604–3630.